

Northumbria Research Link

Citation: Thai, Huu-Tai and Vo, Thuc (2012) Bending and free vibration of functionally graded beams using various higher-order shear deformation beam theories. International Journal of Mechanical Sciences, 62 (1). 57 - 66. ISSN 0020-7403

Published by: Elsevier

URL: <http://dx.doi.org/10.1016/j.ijmecsci.2012.05.014>
<<http://dx.doi.org/10.1016/j.ijmecsci.2012.05.014>>

This version was downloaded from Northumbria Research Link:
<http://nrl.northumbria.ac.uk/id/eprint/13388/>

Northumbria University has developed Northumbria Research Link (NRL) to enable users to access the University's research output. Copyright © and moral rights for items on NRL are retained by the individual author(s) and/or other copyright owners. Single copies of full items can be reproduced, displayed or performed, and given to third parties in any format or medium for personal research or study, educational, or not-for-profit purposes without prior permission or charge, provided the authors, title and full bibliographic details are given, as well as a hyperlink and/or URL to the original metadata page. The content must not be changed in any way. Full items must not be sold commercially in any format or medium without formal permission of the copyright holder. The full policy is available online: <http://nrl.northumbria.ac.uk/policies.html>

This document may differ from the final, published version of the research and has been made available online in accordance with publisher policies. To read and/or cite from the published version of the research, please visit the publisher's website (a subscription may be required.)



**Northumbria
University**
NEWCASTLE



UniversityLibrary

Bending and free vibration of functionally graded beams using various higher-order shear deformation beam theories

Huu-Tai Thai ^{a,*}, Thuc P. Vo ^{b,c}

^a Department of Civil and Environmental Engineering, Hanyang University, 17 Haengdang-dong, Seongdong-gu, Seoul 133-791, Republic of Korea

^b School of Engineering, Glyndwr University, Mold Road, Wrexham LL11 2AW, UK.

^c Advanced Composite Training and Development Centre, Glyndwr University, Unit 5, Hawarden Industrial Park, Deeside, Flintshire CH5 3US, UK.

Abstract

In this paper, various higher-order shear deformation beam theories for bending and free vibration of functionally graded beams are developed. The developed theories account for higher-order variation of transverse shear strain through the depth of the beam, and satisfy the stress-free boundary conditions on the top and bottom surfaces of the beam. A shear correction factor, therefore, is not required. In addition, these theories have strong similarities with Euler-Bernoulli beam theory in some aspects such as equations of motion, boundary conditions, and stress resultant expressions. The material properties of the functionally graded beam are assumed to vary according to power law distribution of the volume fraction of the constituents. Equations of motion and boundary conditions are derived from Hamilton's principle. Analytical solutions are presented, and the obtained results are compared with the existing solutions to verify the validity of the developed theories. Finally, the influences of power law index and shear deformation on the bending and free vibration responses of functionally graded beams are investigated.

Keywords: Functionally graded beam; Higher-order beam theory; Bending; Vibration

* Corresponding author. Tel.: + 82 2 2220 4154.

E-mail address: thaihuutai@hanyang.ac.kr (H.T. Thai), t.vo@glyndwr.ac.uk (T.P. Vo).

1. Introduction

Functionally graded materials (FGMs) are a class of composites that have continuous variation of material properties from one surface to another and thus eliminate the stress concentration at the interface of the layers found in laminated composites. Typically, a FGM is made from a mixture of a ceramic and a metal in such a way that the ceramic can resist high temperature in thermal environments, whereas the metal can decrease the tensile stress occurring on the ceramic surface at the earlier state of cooling. The FGMs are widely used in mechanical, aerospace, nuclear, and civil engineering.

Due to increasing of FGM applications in engineering structures, many beam theories have been developed to predict the response of functionally graded (FG) beams. The classical beam theory (CBT) known as Euler-Bernoulli beam theory is the simplest one and is applicable to slender FG beams only. For moderately deep FG beams, the CBT underestimates deflection and overestimates natural frequency due to ignoring the transverse shear deformation effect [1-3]. The first-order shear deformation beam theory (FBT) known as Timoshenko beam theory has been proposed to overcome the limitations of the CBT by accounting for the transverse shear deformation effect. Since the FBT violates the zero shear stress conditions on the top and bottom surfaces of the beam, a shear correction factor is required to account for the discrepancy between the actual stress state and the assumed constant stress state [4-7]. To avoid the use of a shear correction factor and have a better prediction of response of FG beams, higher-order shear deformation theories have been proposed, notable among them are the third-order theory of Reddy [8-12], the sinusoidal theory of Touratier [13], the hyperbolic theory of Soldatos [14], the exponential theory of Karama et al. [15], and the unified formulation of Carrera [16-17]. Higher-order shear deformation theories can be developed based on

the assumption of a higher-order variation of axial displacement through the depth of the beam [18-24] or both axial and transverse displacements through the depth of the beam (i.e. via the use of a unified formulation) [25-27].

In this paper, various higher-order shear deformation beam theories for bending and free vibration of FG beams are developed based on the assumption of a constant transverse displacement and higher-order variation of axial displacement through the depth of the beam. The proposed theories satisfy the zero traction boundary conditions on the top and bottom surfaces of the beam, thus a shear correction factor is not required. In addition, these theories have strong similarities with the CBT in many aspects such as equations of motion, boundary conditions, and stress resultant expressions. Material properties of FG beams are assumed to vary according to a power law distribution of the volume fraction of the constituents. Equations of motion and boundary conditions are derived from Hamilton's principle. Analytical solutions for bending and free vibration are obtained for a simply supported beam. Numerical examples are presented to show the validity and accuracy of present shear deformation theories. The effects of power law index and shear deformation on the bending and free vibration responses of FG beams are investigated.

2. Kinematics

Consider a functionally graded beam with length L and rectangular cross section $b \times h$, with b being the width and h being the height. The x -, y -, and z -coordinates are taken along the length, width, and height of the beam, respectively, as shown in Fig. 1. The formulation is limited to linear elastic material behavior. The displacement fields of various shear deformation beam theories are chosen based on following assumptions: (1) the axial and transverse displacements are partitioned into bending and shear

components; (2) the bending component of axial displacement is similar to that given by the CBT; and (3) the shear component of axial displacement gives rise to the higher-order variation of shear strain and hence to shear stress through the depth of the beam in such a way that shear stress vanishes on the top and bottom surfaces. Based on these assumptions, the displacement fields of various higher-order shear deformation beam theories are given in a general form as

$$\begin{aligned} u_1(x, z, t) &= u(x, t) - z \frac{dw_b}{dx} - f(z) \frac{dw_s}{dx} \\ u_2(x, z, t) &= 0 \\ u_3(x, z, t) &= w_b(x, t) + w_s(x, t) \end{aligned} \quad (1)$$

where u is the axial displacement of a point on the midplane of the beam; w_b and w_s are the bending and shear components of transverse displacement of a point on the midplane of the beam; and $f(z)$ is a shape function determining the distribution of the transverse shear strain and shear stress through the depth of the beam. The shape functions $f(z)$ are chosen to satisfy the stress-free boundary conditions on the top and bottom surfaces of the beam, thus a shear correction factor is not required. The displacement fields of the third-order beam theory (TBT) based on Reddy [8], sinusoidal beam theory (SBT) based on Touratier [13], hyperbolic beam theory (HBT) based on Soldatos [14], and exponential beam theory (EBT) based on Karama et al. [15] can be obtained from Eq. (1) by using different shape functions $f(z)$ given in Table 1.

Noted that the displacement fields of the proposed theories are different with those of the existing higher-order theories such as TBT [8], SBT [13], HBT [14], and EBT [15]. In the proposed theories, the transverse displacement u_3 is partitioned into the bending and shear parts components (see Eq. (1)), whereas the transverse displacement of the above-mentioned theories is not partitioned into the bending and shear parts. The

partition of transverse displacement into the bending and shear parts helps one to see the contributions due to shear and bending to the total transverse displacement.

The nonzero strains are given by

$$\gamma_x = \frac{du}{dx} - z \frac{d^2 w_b}{dx^2} - f \frac{d^2 w_s}{dx^2} \quad (2a)$$

$$\gamma_{xz} = \left(1 - \frac{df}{dz}\right) \frac{dw_s}{dx} \equiv g \frac{dw_s}{dx} \quad (2b)$$

where $g(z) = 1 - df/dz$ are the shape functions of the transverse shear strains given in Table 1 for various beam models. These shape functions represent the distribution of the transverse shear strains, and hence the transverse shear stresses, through the depth of the beam. Fig. 2 illustrates the transverse shear strain shape function of different models. It is shown that the distribution of transverse shear strain is approximately parabolic, thus satisfying the zero shear stress conditions on the top and bottom surfaces of the beam.

3. Equations of motion

Hamilton's principle is used herein to derive the equations of motion. The principle can be stated in analytical form as [28]

$$0 = \int_{t_1}^{t_2} (\delta U + \delta V - \delta K) dt \quad (3)$$

where t is the time; t_1 and t_2 are the initial and end time, respectively; δU is the virtual variation of the strain energy; δV is the virtual variation of the potential energy; and δK is the virtual variation of the kinetic energy. The variation of the strain energy of the beam can be stated as

$$\delta U = \int_0^L \int_A (\delta \gamma_x \sigma_x + \delta \gamma_{xz} \tau_{xz}) dA dx = \int_0^L \left(N \frac{du}{dx} - M_b \frac{d^2 u}{dx^2} - M_s \frac{d^2 w_s}{dx^2} + Q \frac{dw_s}{dx} \right) dx \quad (4)$$

where N , M , and Q are the stress resultants defined as

$$N = \int_A \dagger_x dA \quad (5a)$$

$$M_b = \int_A z \dagger_x dA \quad (5b)$$

$$M_s = \int_A f \dagger_x dA \quad (5c)$$

$$Q = \int_A g \dagger_{xz} dA \quad (5d)$$

The variation of the potential energy by the applied transverse load q can be written as

$$\delta V = - \int_0^L q \delta u (w_b + w_s) dx \quad (6)$$

The variation of the kinetic energy can be expressed as

$$\begin{aligned} \delta K &= \int_0^L \int_A \dots(z) (\dot{\delta u}_1 \dot{u}_1 + \dot{\delta u}_2 \dot{u}_2 + \dot{\delta u}_3 \dot{u}_3) dA dx \\ &= \int_0^L \left\{ I_0 \left[\dot{\delta u} \dot{u} + (\dot{w}_b + \dot{w}_s) \delta u (\dot{w}_b + \dot{w}_s) \right] - I_1 \left(\dot{u} \frac{d \dot{w}_b}{dx} + \frac{d \dot{w}_b}{dx} \delta u \dot{u} \right) + I_2 \frac{d \dot{w}_b}{dx} \frac{d \delta u \dot{w}_b}{dx} \right. \\ &\quad \left. - J_1 \left(\dot{u} \frac{d \dot{w}_s}{dx} + \frac{d \dot{w}_s}{dx} \delta u \dot{u} \right) + K_2 \frac{d \dot{w}_s}{dx} \frac{d \delta u \dot{w}_s}{dx} + J_2 \left(\frac{d \dot{w}_b}{dx} \frac{d \delta u \dot{w}_s}{dx} + \frac{d \dot{w}_s}{dx} \frac{d \delta u \dot{w}_b}{dx} \right) \right\} dx \end{aligned} \quad (7)$$

where dot-superscript convention indicates the differentiation with respect to the time variable t ; $\dots(z)$ is the mass density; and $(I_0, I_1, J_1, I_2, J_2, K_2)$ are the mass inertias defined as

$$I_0 = \int_A \dots(z) dA \quad (8a)$$

$$I_1 = \int_A z \dots(z) dA \quad (8b)$$

$$J_1 = \int_A f \dots(z) dA \quad (8c)$$

$$I_2 = \int_A z^2 \dots(z) dA \quad (8d)$$

$$J_2 = \int_A z f \dots(z) dA \quad (8e)$$

$$K_2 = \int_A f^2 \dots(z) dA \quad (8f)$$

Substituting the expressions for uU , uV , and uK from Eqs. (4), (6), and (7) into Eq. (3) and integrating by parts versus both space and time variables, and collecting the coefficients of uu , uw_b , and uw_s , the following equations of motion of the functionally graded beam are obtained

$$uu : \frac{dN}{dx} = I_0 \ddot{u} - I_1 \frac{d\ddot{w}_b}{dx} - J_1 \frac{d\ddot{w}_s}{dx} \quad (9a)$$

$$uw_b : \frac{d^2 M_b}{dx^2} + q = I_0 (\ddot{w}_b + \ddot{w}_s) + I_1 \frac{d\ddot{u}}{dx} - I_2 \frac{d^2 \ddot{w}_b}{dx^2} - J_2 \frac{d^2 \ddot{w}_s}{dx^2} \quad (9b)$$

$$uw_s : \frac{d^2 M_s}{dx^2} + \frac{dQ}{dx} + q = I_0 (\ddot{w}_b + \ddot{w}_s) + J_1 \frac{d\ddot{u}}{dx} - J_2 \frac{d^2 \ddot{w}_b}{dx^2} - K_2 \frac{d^2 \ddot{w}_s}{dx^2} \quad (9c)$$

The boundary conditions are of the form: specify

$$u \text{ or } N \quad (10a)$$

$$w_b \text{ or } Q_b \equiv \frac{dM_b}{dx} - I_1 \ddot{u} + I_2 \frac{d\ddot{w}_b}{dx} + J_2 \frac{d\ddot{w}_s}{dx} \quad (10b)$$

$$w_s \text{ or } Q_s \equiv \frac{dM_s}{dx} + Q - J_1 \ddot{u} + J_2 \frac{d\ddot{w}_b}{dx} + K_2 \frac{d\ddot{w}_s}{dx} \quad (10c)$$

$$\frac{dw_b}{dx} \text{ or } M_b \quad (10d)$$

$$\frac{dw_s}{dx} \text{ or } M_s \quad (10e)$$

The equations of motion and boundary conditions of the CBT can be obtained from Eqs. (9) and (10) by setting the shear component of transverse displacement w_s equal to zero.

4. Constitutive equations

FGMs are composite materials made of ceramic and metal. The material properties of FG beams are assumed to vary continuously through the depth of the beam by a power

law as [19, 22, 24, 29]

$$P(z) = P_m + (P_c - P_m)V_c, \quad V_c = \left(\frac{1}{2} + \frac{z}{h}\right)^p \quad \text{and} \quad V_m = 1 - V_c \quad (11)$$

where P represents the effective material property such as Young's modulus E , Poisson's ratio ϵ , and mass density ρ ; subscripts m and c represent the metallic and ceramic constituents, respectively; and p is the power law index which governs the volume fraction gradation. Fig. 3 illustrates the variation of the volume fraction V_c through the depth of the beam for various values of the power law index. The value of p equal to zero represents a fully ceramic beam, whereas infinite p indicates a fully metallic beam. The variation of the combination of ceramic and metal is linear for $p = 1$.

The linear constitutive relations of a FG beam can be written as

$$\tau_x = Q_{11}(z)\nu_x \quad (12a)$$

$$\tau_{xz} = Q_{55}(z)\chi_{xz} \quad (12b)$$

where

$$Q_{11}(z) = E(z) \quad (13a)$$

$$Q_{55}(z) = \frac{E(z)}{2[1 + \epsilon(z)]} \quad (13b)$$

By substituting Eq. (2) into Eq. (12) and the subsequent results into Eq. (5), the constitutive equations for the stress resultants are obtained as

$$N = A \frac{du}{dx} - B \frac{d^2 w_b}{dx^2} - B_s \frac{d^2 w_s}{dx^2} \quad (14a)$$

$$M_b = B \frac{du}{dx} - D \frac{d^2 w_b}{dx^2} - D_s \frac{d^2 w_s}{dx^2} \quad (14b)$$

$$M_s = B_s \frac{du}{dx} - D_s \frac{d^2 w_b}{dx^2} - H_s \frac{d^2 w_s}{dx^2} \quad (14c)$$

$$Q = A_s \frac{dw_s}{dx} \quad (14d)$$

where

$$A = \int_A Q_{11} dA \quad (15a)$$

$$B = \int_A z Q_{11} dA \quad (15b)$$

$$B_s = \int_A f Q_{11} dA \quad (15c)$$

$$D = \int_A z^2 Q_{11} dA \quad (15d)$$

$$D_s = \int_A z f Q_{11} dA \quad (15e)$$

$$H_s = \int_A f^2 Q_{11} dA \quad (15f)$$

$$A_s = \int_A g^2 Q_{55} dA \quad (15g)$$

5. Equations of motion in terms of displacements

By substituting the stress resultants in Eq. (14) into Eq. (9), the equations of motion can be expressed in terms of displacements (u, w_b, w_s) as

$$A \frac{d^2 u}{dx^2} - B \frac{d^3 w_b}{dx^3} - B_s \frac{d^3 w_s}{dx^3} = I_0 \ddot{u} - I_1 \frac{d \ddot{w}_b}{dx} - J_1 \frac{d \ddot{w}_s}{dx} \quad (16a)$$

$$B \frac{d^3 u}{dx^3} - D \frac{d^4 w_b}{dx^4} - D_s \frac{d^4 w_s}{dx^4} + q = I_0 (\ddot{w}_b + \ddot{w}_s) + I_1 \frac{d \ddot{u}}{dx} - I_2 \frac{d^2 \ddot{w}_b}{dx^2} - J_2 \frac{d^2 \ddot{w}_s}{dx^2} \quad (16b)$$

$$B_s \frac{d^3 u}{dx^3} - D_s \frac{d^4 w_b}{dx^4} - H_s \frac{d^4 w_s}{dx^4} + A_s \frac{d^2 w_s}{dx^2} + q = I_0 (\ddot{w}_b + \ddot{w}_s) + J_1 \frac{d \ddot{u}}{dx} - J_2 \frac{d^2 \ddot{w}_b}{dx^2} - K_2 \frac{d^2 \ddot{w}_s}{dx^2} \quad (16c)$$

6. Analytical solutions

The above equations of motion are analytically solved for bending and free vibration problems. The Navier solution procedure is used to determine the analytical solutions

for a simply supported beam. The solution is assumed to be of the form

$$\begin{aligned} u(x, t) &= \sum_{n=1}^{\infty} U_n e^{i\tilde{S}_t} \cos \Gamma x \\ w_b(x, t) &= \sum_{n=1}^{\infty} W_{bn} e^{i\tilde{S}_t} \sin \Gamma x \\ w_s(x, t) &= \sum_{n=1}^{\infty} W_{sn} e^{i\tilde{S}_t} \sin \Gamma x \end{aligned} \quad (17)$$

where $i = \sqrt{-1}$, $\Gamma = n\pi / L$, (U_n, W_{bn}, W_{sn}) are the unknown maximum displacement coefficients, and \tilde{S} is the natural frequency. The transverse load q is also expanded in Fourier series as

$$q(x) = \sum_{n=1}^{\infty} Q_n \sin \Gamma x \quad (18)$$

where Q_n is the load amplitude calculated from

$$Q_n = \frac{2}{L} \int_0^L q(x) \sin \Gamma x dx \quad (19)$$

The coefficients Q_n are given below for some typical loads

$$Q_n = \begin{cases} q_0 & (n=1) & \text{for sinusoidal load } q_0 \\ \frac{4q_0}{n\pi} & (n=1, 3, 5, \dots) & \text{for uniform load } q_0 \\ \frac{2}{L} Q_0 \sin \frac{n\pi}{2} & (n=1, 2, 3, \dots) & \text{for point load } Q_0 \text{ at the center} \end{cases} \quad (20)$$

Substituting the expansions of u , w_b , w_s , and q from Eqs. (17) and (18) into the equations of motion Eq. (16), the analytical solutions can be obtained from the following equations

$$\begin{pmatrix} s_{11} & s_{12} & s_{13} \\ s_{12} & s_{22} & s_{23} \\ s_{13} & s_{23} & s_{33} \end{pmatrix} - \tilde{S}^2 \begin{pmatrix} m_{11} & m_{12} & m_{13} \\ m_{12} & m_{22} & m_{23} \\ m_{13} & m_{23} & m_{33} \end{pmatrix} \begin{Bmatrix} U_n \\ W_{bn} \\ W_{sn} \end{Bmatrix} = \begin{Bmatrix} 0 \\ Q_n \\ Q_n \end{Bmatrix} \quad (21)$$

where

$$\begin{aligned} s_{11} &= A r^2, s_{12} = -B r^3, s_{13} = -B_s r^3, s_{22} = D r^4, s_{23} = D_s r^4, s_{33} = H_s r^4 + A_s r^2 \\ m_{11} &= I_0, m_{12} = -I_1 r, m_{13} = -J_1 r, m_{22} = I_0 + I_2 r^2, m_{23} = I_0 + J_2 r^2, m_{33} = I_0 + K_2 r^2 \end{aligned} \quad (22)$$

7. Results and discussion

In this section, various numerical examples are presented and discussed to verify the accuracy of present theories in predicting the bending and free vibration responses of simply supported FG beams. For numerical results, an Al/Al₂O₃ beam composed of aluminum (as metal) and alumina (as ceramic) is considered. The material properties of aluminum are $E_m = 70$ GPa, $\epsilon_m = 0.30$, and $\rho_m = 2702$ kg/m³, and those of alumina are $E_c = 380$ GPa, $\epsilon_c = 0.3$, and $\rho_c = 3960$ kg/m³ [23]. For convenience, the following dimensionless forms are used:

$$\begin{aligned} \bar{w} &= 100 \frac{E_m h^3}{q_0 L^4} w \left(\frac{L}{2} \right), \bar{u} = 100 \frac{E_m h^3}{q_0 L^4} u \left(0, -\frac{h}{2} \right) \\ \bar{\tau}_x &= \frac{h}{q_0 L} \tau_x \left(\frac{L}{2}, \frac{h}{2} \right), \bar{\tau}_{xz} = \frac{h}{q_0 L} \tau_{xz} (0, 0), \bar{\zeta} = \frac{\zeta L^2}{h} \sqrt{\frac{\rho_m}{E_m}} \end{aligned} \quad (23)$$

7.1. Results for bending analysis

Table 2 contains the nondimensional deflections and stresses of FG beams under uniform load q_0 for different values of power law index p and span-to-depth ratio L/h . The calculated values based on the present TBT, SBT, HBT, EBT, and CBT are obtained using 100 terms in series in Eq. (20). It is worth noting that the results of Li et al. [22] are evaluated based on the analytical solutions given in the Appendix B in the Ref. [22]. It can be observed that the values obtained using various shear deformation beam theories (i.e., TBT, SBT, HBT, and EBT) are in good agreement with the those given by Li et al. [22] for all values of power law index p and span-to-depth ratio L/h . Due to ignoring the shear deformation effect, CBT underestimates deflection of

moderately deep beams ($L/h = 5$). The maximum difference in transverse deflection between CBT and shear deformation beam theories is 13% for $p = 10$. Figs. 4-6 show the variations of axial displacement \bar{u} , axial stress $\bar{\tau}_x$, and transverse shear stress $\bar{\tau}_{xz}$, respectively, through the depth of a very deep beam ($L = 2h$) under uniform load. In general, all shear deformation beam models give almost identical results, except for the case of transverse shear stress $\bar{\tau}_{xz}$. It can be explained by the different transverse shear strain shape functions $g(z)$ used in each models (see Fig. 2).

To illustrate the effect of power law index p on the bending response of FG beams under uniform load, the axial displacement \bar{u} , transverse deflection \bar{w} , and axial stress $\bar{\tau}_x$, respectively are plotted in Figs. 7-9. Since there are no differences between the results of shear deformation beam theories, TBT is used only in Figs. 7-9. It can be seen that increasing the power law index p will reduce the stiffness of the FG beams, and consequently, leads to an increase in the deflections and axial stress. This is due to the fact that higher values of power law index p correspond to high portion of metal in comparison with the ceramic part, thus makes such FG beams more flexible. The effect of shear deformation on deflection of FG beams is shown in Fig. 10 for various values of power law index p . In this figure, the deflection ratio is defined as the ratio of deflection predicted by shear deformation beam theory to that predicted by CBT. It can be seen that the deflection ratio is greater than unity, as expected. It means that the inclusion of shear deformation effect leads to an increase in the deflections and more pronounced for short beams.

7.2. Results for free vibration analysis

Table 3 shows the nondimensional fundamental frequencies \tilde{S} of FG beams for

different values of power law index p and span-to-depth ratio L/h . The calculated frequencies are compared with those given by Simsek [23] using various beam theories. It should be noted that the results reported by Simsek [23] based on various shear deformation beam models in which the shear strains are approximated in terms of shear rotations instead of shear components of bending rotation as in this study. An excellent agreement between the present solutions and results of Simsek [23] is found. The first three nondimensional frequencies $\tilde{\omega}$ of FG beams predicted by various proposed beam models are presented in Table 4 for different values of power law index p and span-to-depth ratio L/h . It can be seen that all shear deformation beam theories give the same frequencies, whereas the CBT overestimates them for all cases considered. Effect of shear deformation on frequency ratio, which is defined as the ratio of frequency predicted by shear deformation beam theory to that predicted by CBT, is plotted in Fig. 11. The difference between the frequencies of CBT and shear deformation beam theories is significant for higher modes and for small span-to-depth ratios L/h (see Table 4 and Fig. 11). This is due to the effects of shear deformation and rotary inertia. These effects lead to a reduction of the vibration frequencies and the reduction is amplified at higher vibration modes and for small span-to-depth ratios. It implies that shear deformation beam models should be employed for a better prediction of the frequencies instead of CBT which neglects the effects of transverse shear deformation and rotary inertia. The corresponding three mode shapes are also plotted in Fig. 12 for homogeneous and FG beams ($L = 5h$). Relative measures of the axial and flexural displacements show that for homogeneous material, vibration modes exhibit double coupled mode (bending and shear components), whereas, for FG material, the beam displays one further mode (axial mode). The resulting mode shape is referred to as triply

axial-flexural coupled mode.

The effect of power law index p on the frequency of FG beams is shown in Fig. 13. It is observed that an increase in the value of the power law index leads to a reduction of frequency. The highest frequency values are obtained for full ceramic beams ($p = 0$) while the lowest frequency values are obtained for full metal beams ($p \rightarrow \infty$). This is due to the fact that an increase in the value of the power law index results in a decrease in the value of elasticity modulus. In other words, the beam becomes flexible as the power law index increases, thus decreasing the frequency values.

8. Conclusions

Various higher-order shear deformation beam theories for bending and free vibration of FG beams are developed. The displacement fields of the proposed beam theories are chosen based on the assumption of a constant transverse displacement and higher-order variation of axial displacement through the depth of the beam. Equations of motion are derived from Hamilton's principle. Analytical solutions are obtained for a simply supported beam. Effects of power law index and shear deformation on the bending and free vibration responses of FG beams are investigated. The following points can be outlined from the present study:

- (1) The proposed beam theories satisfy the stress-free boundary conditions on the top and bottom surfaces of the beam, and do not require a shear correction factor.
- (2) CBT comes out as a special case of the proposed theories. Hence, finite element modes based on these beam theories will be free from shear locking.
- (3) The results of all proposed beam theories are almost identical to each other, and agree well with the existing solutions.
- (4) Increasing the power law index will reduce the stiffness of FG beam, and consequently,

leads to an increase in the deflections and a reduction of the natural frequencies.

- (5) The inclusion of the shear deformation effects leads to an increase in the deflections and a reduction of the natural frequencies.

References

- [1] Yang J, Chen Y. Free vibration and buckling analyses of functionally graded beams with edge cracks. *Composite Structures* 2008;83(1):48-60.
- [2] Simsek M, Kocaturk T. Free and forced vibration of a functionally graded beam subjected to a concentrated moving harmonic load. *Composite Structures* 2009;90(4):465-473.
- [3] Alshorbagy AE, Eltaher M, Mahmoud F. Free vibration characteristics of a functionally graded beam by finite element method. *Applied Mathematical Modelling* 2011;35(1):412-425.
- [4] Chakraborty A, Gopalakrishnan S, Reddy JN. A new beam finite element for the analysis of functionally graded materials. *International Journal of Mechanical Sciences* 2003;45(3):519-539.
- [5] Li XF. A unified approach for analyzing static and dynamic behaviors of functionally graded Timoshenko and Euler–Bernoulli beams. *Journal of Sound and Vibration* 2008;318(4–5):1210-1229.
- [6] Sina SA, Navazi HM, Haddadpour H. An analytical method for free vibration analysis of functionally graded beams. *Materials and Design* 2009;30(3):741-747.
- [7] Wei D, Liu Y, Xiang Z. An analytical method for free vibration analysis of functionally graded beams with edge cracks. *Journal of Sound and Vibration* 2012;331(7):1686-1700.
- [8] Reddy JN. A simple higher-order theory for laminated composite plates. *Journal of*

Applied Mechanics 1984;51(4):745-752.

- [9] Wang CM, Reddy JN, Lee KH. Shear deformable beams and plates: Relationships with classical solutions: Elsevier Science; 2000.
- [10] Yesilce Y, Catal S. Free vibration of axially loaded Reddy-Bickford beam on elastic soil using the differential transform method. Structural Engineering and Mechanics 2009;31(4):453-476.
- [11] Yesilce Y. Effect of axial force on the free vibration of Reddy-Bickford multi-span beam carrying multiple spring-mass systems. Journal of Vibration and Control 2010;16(1):11-32.
- [12] Yesilce Y, Catal HH. Solution of free vibration equations of semi-rigid connected Reddy-Bickford beams resting on elastic soil using the differential transform method. Archive of Applied Mechanics 2011;81(2):199-213.
- [13] Touratier M. An efficient standard plate theory. International Journal of Engineering Science 1991;29(8):901-916.
- [14] Soldatos K. A transverse shear deformation theory for homogeneous monoclinic plates. Acta Mechanica 1992;94(3):195-220.
- [15] Karama M, Afaq KS, Mistou S. Mechanical behaviour of laminated composite beam by the new multi-layered laminated composite structures model with transverse shear stress continuity. International Journal of Solids and Structures 2003;40(6):1525-1546.
- [16] Carrera E. Theories and finite elements for multilayered plates and shells: a unified compact formulation with numerical assessment and benchmarking. Archives of Computational Methods in Engineering 2003;10(3):215-296.
- [17] Carrera E, Giunta G, Petrolo M. Beam structures: classical and advanced theories.

West Sussex, UK: John Wiley & Sons, Ltd; 2011.

- [18] Aydogdu M, Taskin V. Free vibration analysis of functionally graded beams with simply supported edges. *Materials and Design* 2007;28(5):1651-1656.
- [19] Kadoli R, Akhtar K, Ganesan N. Static analysis of functionally graded beams using higher order shear deformation theory. *Applied Mathematical Modelling* 2008;32(12):2509-2525.
- [20] Simsek M. Static analysis of a functionally graded beam under a uniformly distributed load by Ritz method. *International Journal of Engineering and Applied Sciences* 2009;1(3):1-11.
- [21] Sallai BO, Tounsi A, Mechab I, Bouiadjra MB, Meradjah M, Bedia EA. A theoretical analysis of flexional bending of Al/Al₂O₃ S-FGM thick beams. *Computational Materials Science* 2009;44(4):1344-1350.
- [22] Li XF, Wang BL, Han JC. A higher-order theory for static and dynamic analyses of functionally graded beams. *Archive of Applied Mechanics* 2010;80(10):1197-1212.
- [23] Simsek M. Fundamental frequency analysis of functionally graded beams by using different higher-order beam theories. *Nuclear Engineering and Design* 2010;240(4):697-705.
- [24] Wattanasakulpong N, Gangadhara Prusty B, Kelly DW. Thermal buckling and elastic vibration of third-order shear deformable functionally graded beams. *International Journal of Mechanical Sciences* 2011;53(9):734-743.
- [25] Giunta G, Belouettar S, Carrera E. Analysis of FGM beams by means of classical and advanced theories. *Mechanics of Advanced Materials and Structures* 2010;17(8):622-635.
- [26] Giunta G, Belouettar S, Carrera E. Analysis of FGM beams by means of a unified

formulation. IOP Conference Series: Materials Science and Engineering 2010;10:012073.

[27]Giunta G, Crisafulli D, Belouettar S, Carrera E. Hierarchical theories for the free vibration analysis of functionally graded beams. Composite Structures 2011;94(1):68-74.

[28]Reddy JN. Energy principles and variational methods in applied mechanics: John Wiley & Sons Inc; 2002.

[29]Markworth AJ, Ramesh KS, Parks WP. Modelling studies applied to functionally graded materials. Journal of Materials Science 1995;30(9):2183-2193.

Figure Captions

Fig. 1. Geometry and coordinate of a FG beam

Fig. 2. Shear strain shape function of various beam models

Fig. 3. Variation of volume fraction V_c through the depth of a FG beam for various values of the power law index p

Fig. 4. Variation of nondimensional axial displacement $\bar{u}(0, z)$ across the depth of FG beams under uniform load ($L = 2h$)

Fig. 5. Variation of nondimensional axial normal stress $\bar{\tau}_x(L/2, z)$ across the depth of FG beams under uniform load ($L = 2h$)

Fig. 6. Variation of nondimensional transverse shear stress $\bar{\tau}_{xz}(0, z)$ across the depth of FG beams under uniform load ($L = 2h$)

Fig. 7. Variation of nondimensional axial displacement \bar{u} with respect to the power law index p for FG beams under uniform loads

Fig. 8. Variation of nondimensional transverse deflection \bar{w} with respect to the power law index p for FG beams under uniform load

Fig. 9. Variation of nondimensional axial normal stress $\bar{\tau}_x$ with respect to the power law index p for FG beams under uniform load

Fig. 10. Effect of shear deformation and power index p on deflection of FG beams under uniform loads

Fig. 11. Effect of shear deformation and power index p on frequencies of FG beams

Fig. 12. First three mode shapes of FG beams ($L = 5h$)

Fig. 13. Variation of nondimensional fundamental frequency $\bar{\omega}$ with respect to power law index p and span-to-depth ratio L/h of FG beams

Table Captions

Table 1. Shape functions

Table 2. Nondimensional deflections and stresses of FG beams under uniform load

Table 3. Nondimensional fundamental frequency $\tilde{\omega}$ of FG beams

Table 4. First three nondimensional frequencies $\tilde{\omega}$ of FG beams

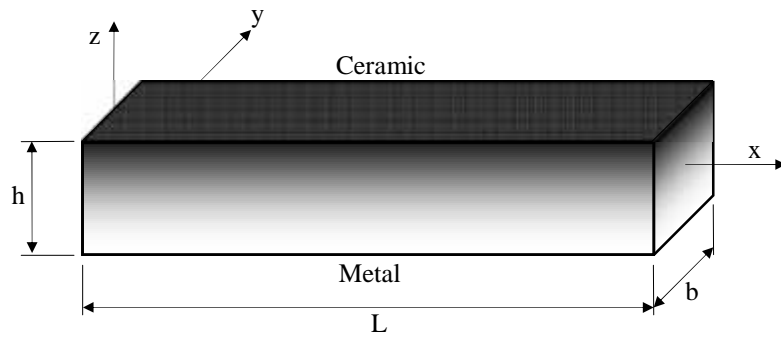


Fig. 1. Geometry and coordinate of a FG beam

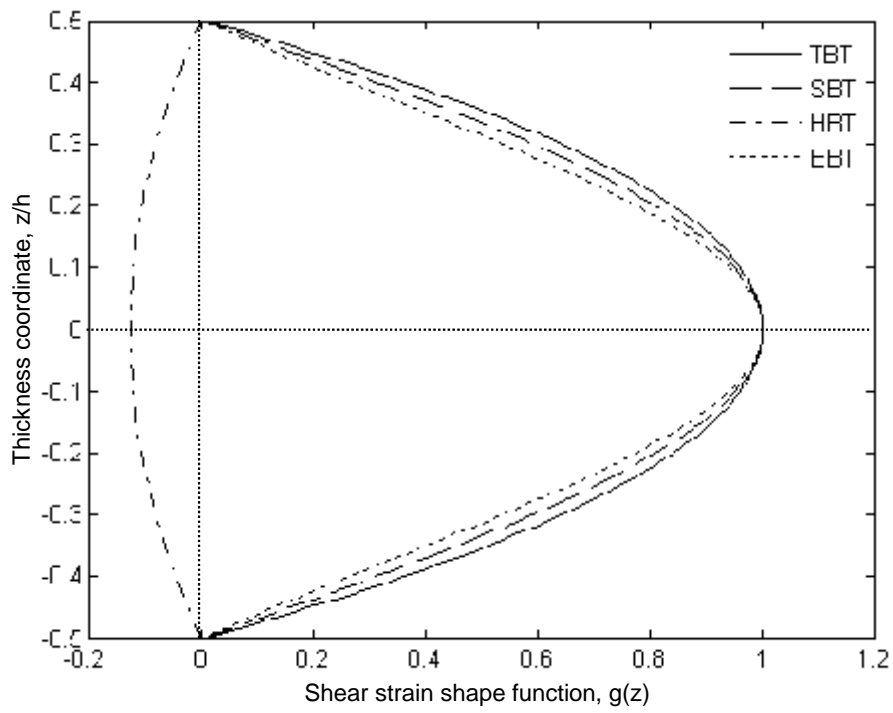


Fig. 2. Shear strain shape function of various beam models

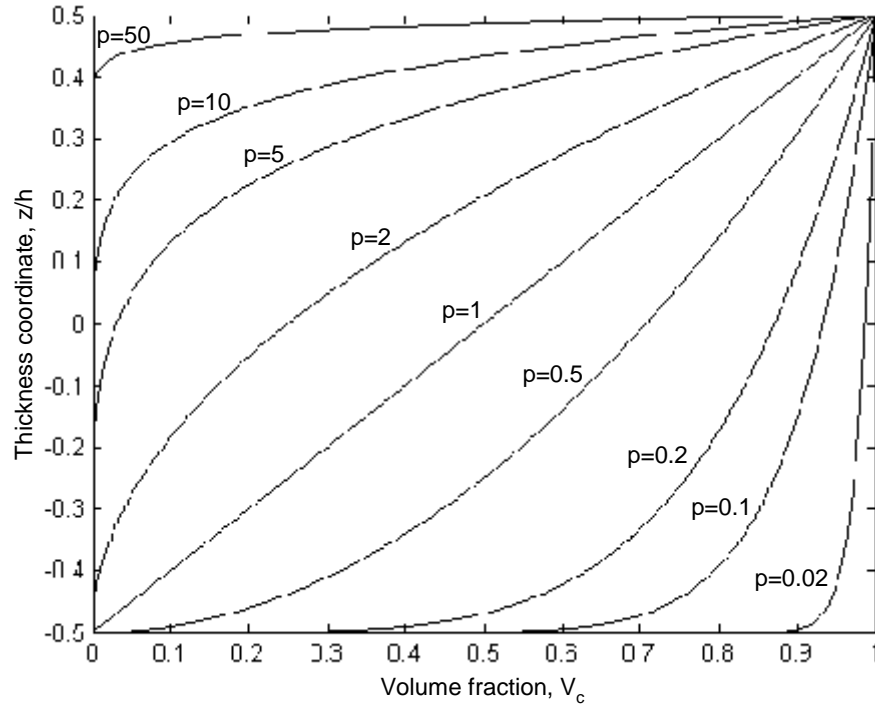
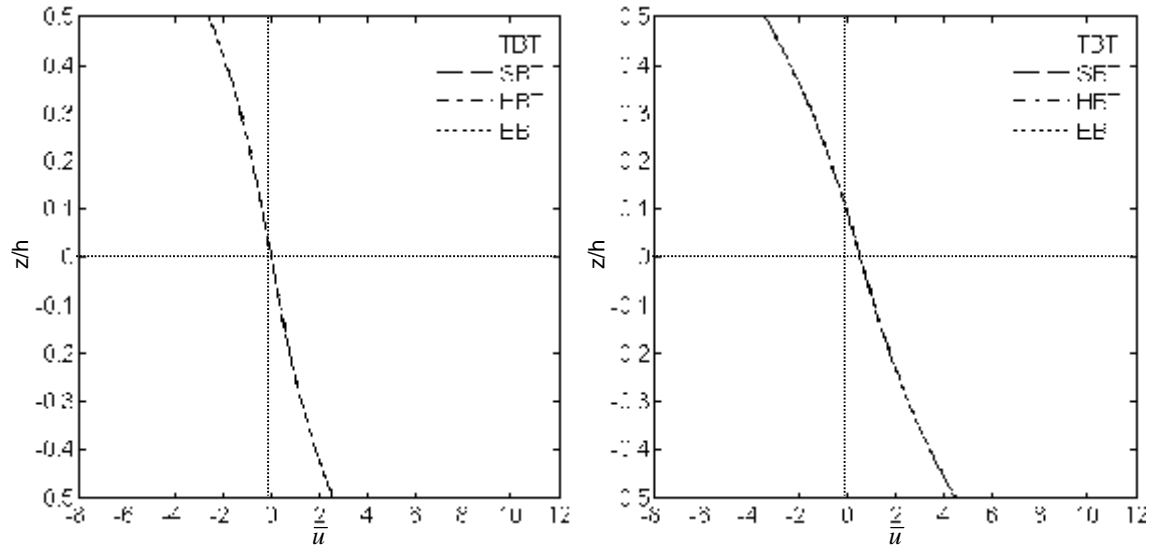
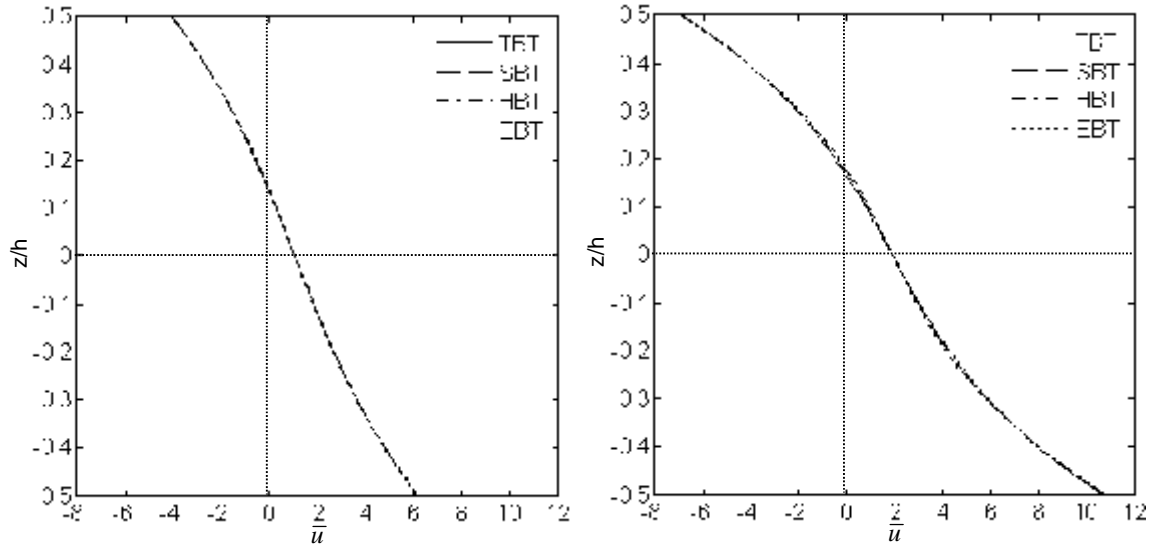


Fig. 3. Variation of volume fraction V_c through the depth of a FG beam for various values of the power law index p



(a) $p=0$

(b) $p=0.5$



(c) $p=1$

(d) $p=10$

Fig. 4. Variation of nondimensional axial displacement $\bar{u}(0, z)$ across the depth of FG beams under uniform load ($L = 2h$)

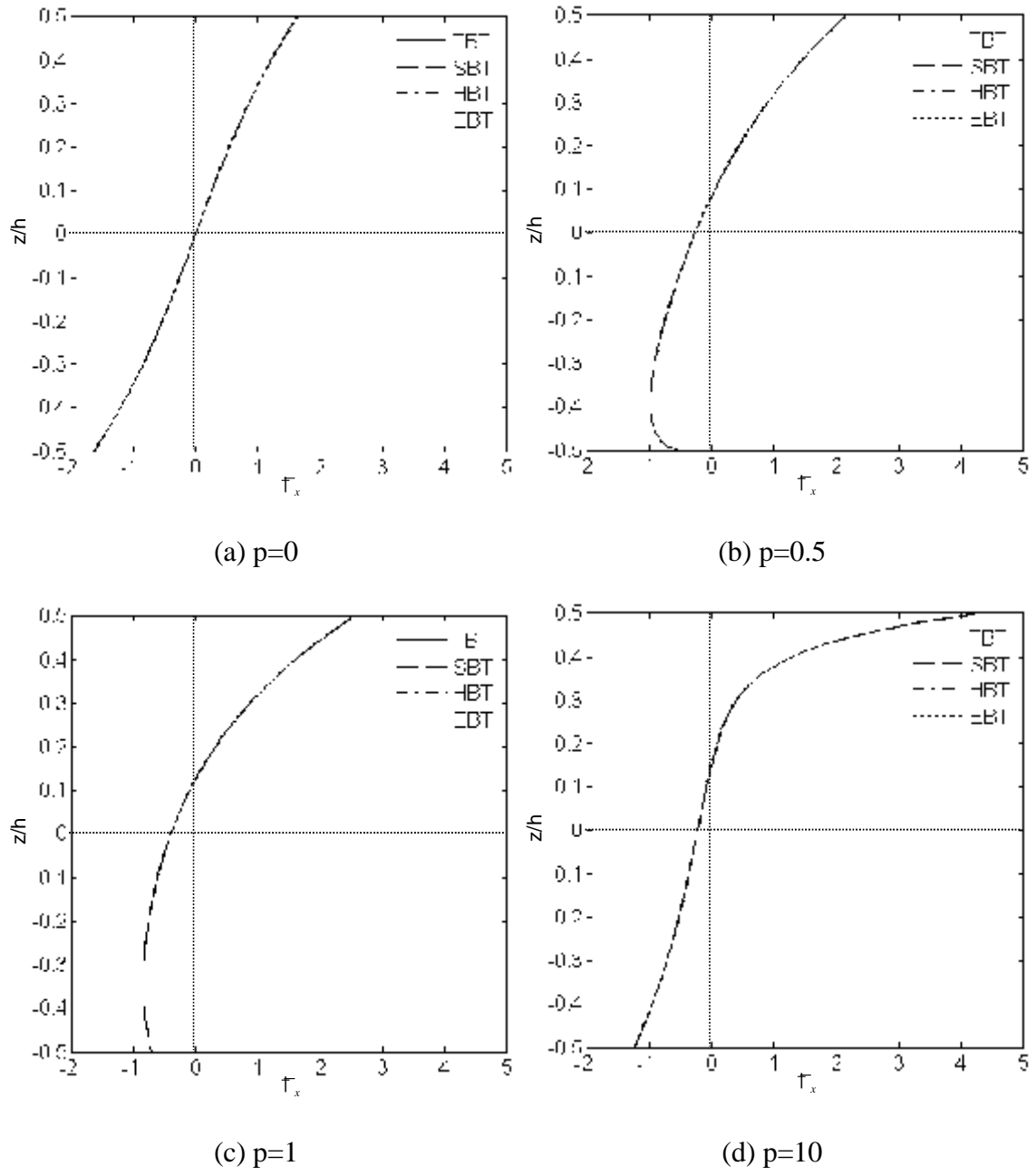


Fig. 5. Variation of nondimensional axial normal stress $\bar{\tau}_x(L/2, z)$ across the depth of FG beams under uniform load ($L = 2h$)

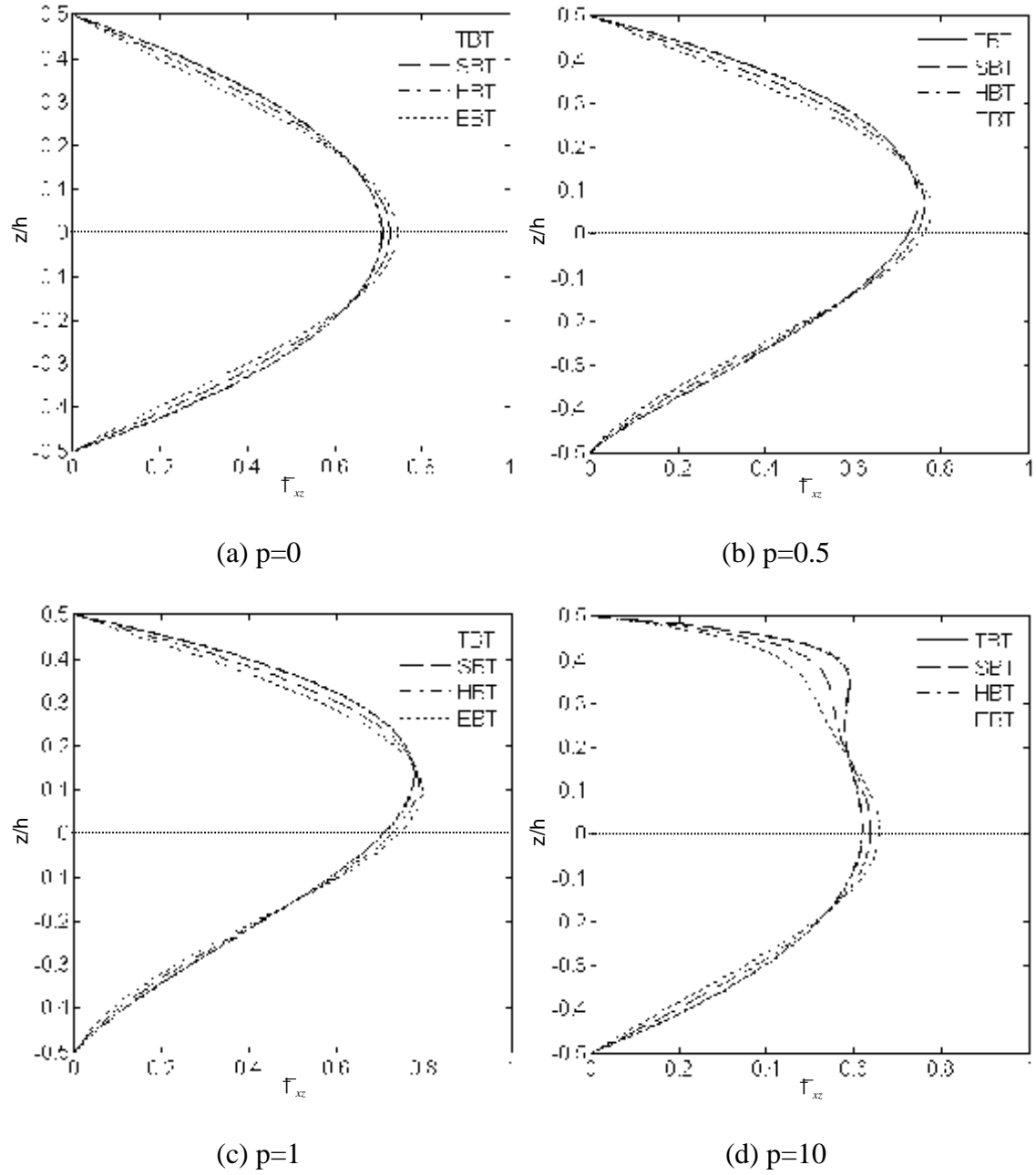


Fig. 6. Variation of nondimensional transverse shear stress $\tau_{xz}(0, z)$ across the depth of FG beams under uniform load ($L = 2h$)

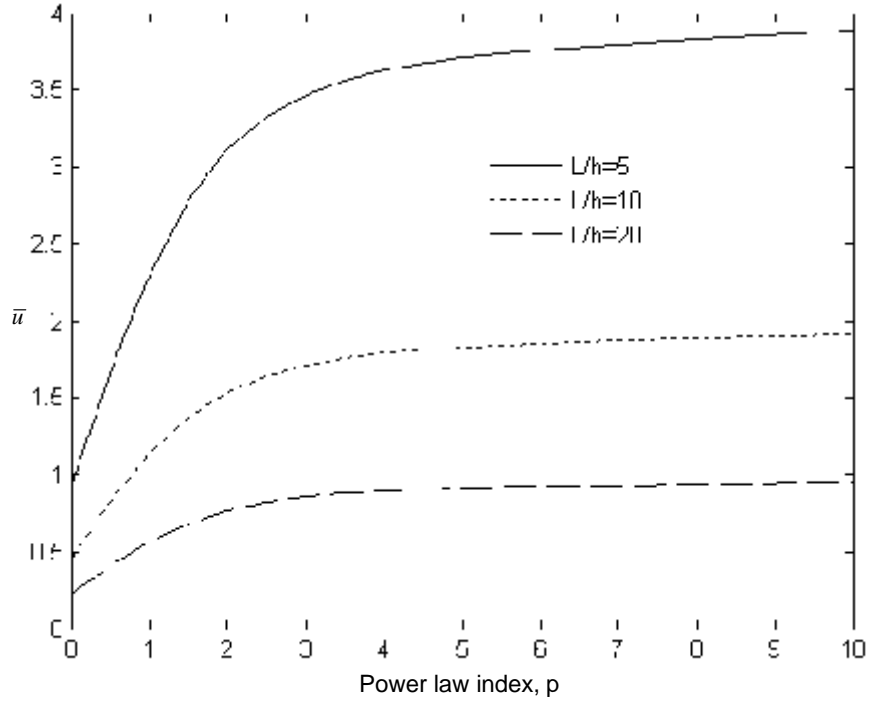


Fig. 7. Variation of nondimensional axial displacement \bar{u} with respect to the power law index p for FG beams under uniform loads

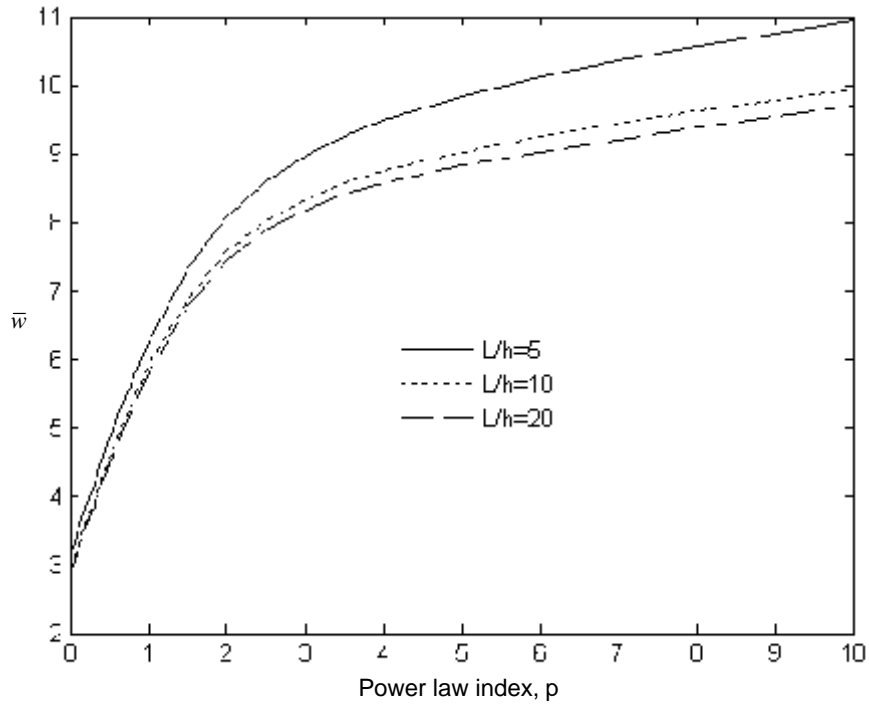


Fig. 8. Variation of nondimensional transverse deflection \bar{w} with respect to the power law index p for FG beams under uniform load

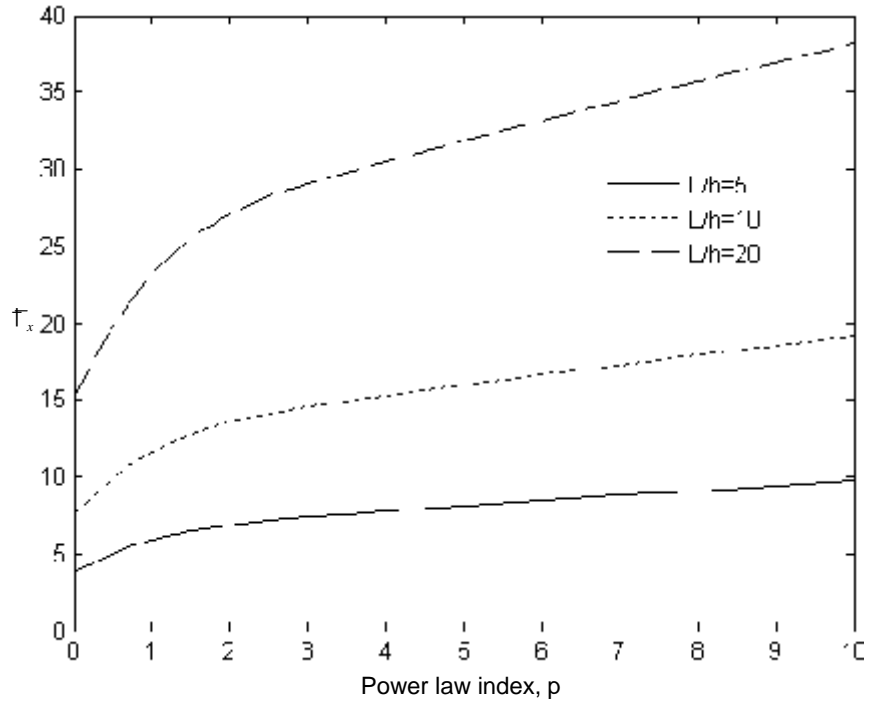


Fig. 9. Variation of nondimensional axial normal stress τ_x with respect to the power law index p for FG beams under uniform load

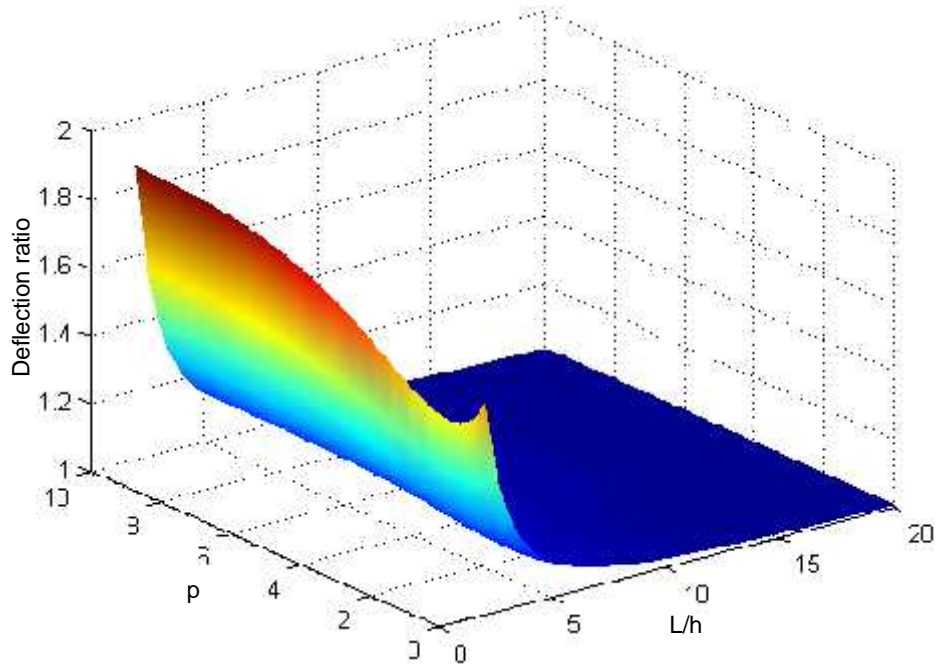


Fig. 10. Effect of shear deformation and power index p on deflection of FG beams under uniform loads

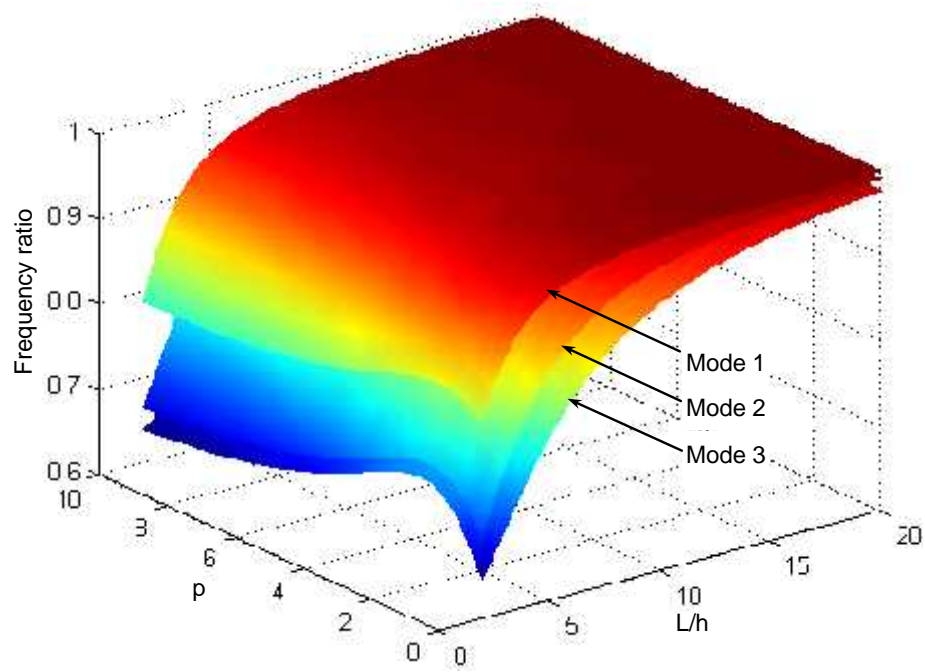
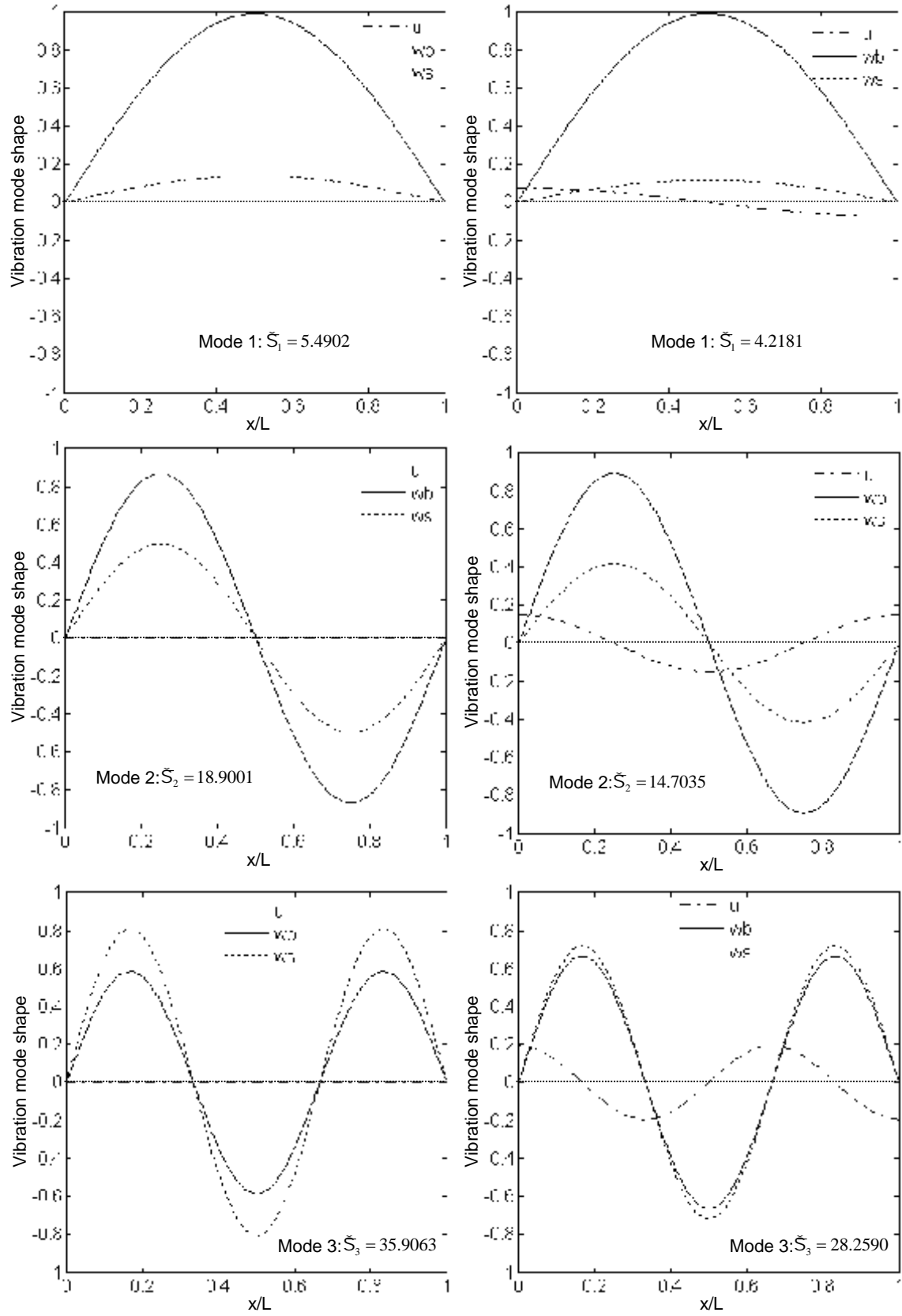


Fig. 11. Effect of shear deformation and power index p on frequencies of FG beams



(a) Homogeneous beam ($p=0$)

(b) Functionally graded beam ($p=1$)

Fig. 12. First three mode shapes of FG beams ($L = 5h$)

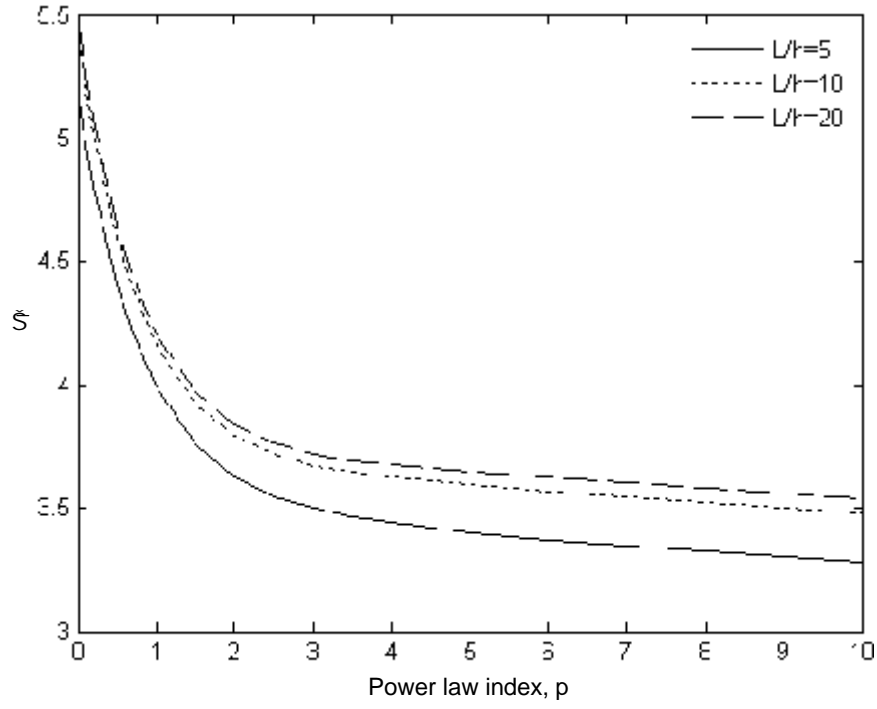


Fig. 13. Variation of nondimensional fundamental frequency \tilde{S} with respect to power law index p and span-to-depth ratio L/h of FG beams

Table 1. Shape functions

Model	$f(z)$	$g(z) = 1 - df/dz$
TBT based on Reddy [8]	$\frac{4z^3}{3h^2}$	$1 - \frac{4z^2}{h^2}$
SBT based on Touratier [13]	$z - \frac{h}{f} \sin\left(\frac{fz}{h}\right)$	$\cos\left(\frac{fz}{h}\right)$
HBT based on Soldatos [14]	$z - h \sinh\left(\frac{z}{h}\right) + z \cosh\frac{1}{2}$	$\cosh\left(\frac{z}{h}\right) - \cosh\frac{1}{2}$
EBT based on Karama et al. [15]	$z - ze^{-2(z/h)^2}$	$\left(1 - \frac{4z^2}{h^2}\right)e^{-2(z/h)^2}$
Classical beam theory (CBT)	z	0

Table 2. Nondimensional deflections and stresses of FG beams under uniform load

p	Method	$L/h = 5$				$L/h = 20$			
		\bar{w}	\bar{u}	\bar{f}_x	\bar{f}_{xz}	\bar{w}	\bar{u}	\bar{f}_x	\bar{f}_{xz}
0	Li et al. [22]	3.1657	0.9402	3.8020	0.7500	2.8962	0.2306	15.0130	0.7500
	TBT	3.1654	0.9398	3.8020	0.7332	2.8962	0.2306	15.0129	0.7451
	SBT	3.1649	0.9409	3.8053	0.7549	2.8962	0.2306	15.0138	0.7686
	HBT	3.1654	0.9397	3.8017	0.7312	2.8962	0.2306	15.0129	0.7429
	EBT	3.1635	0.9420	3.8083	0.7763	2.8961	0.2306	15.0145	0.7920
	CBT	2.8783	0.9211	3.7500	-	2.8783	0.2303	15.0000	-
0.5	Li et al. [22]	4.8292	1.6603	4.9925	0.7676	4.4645	0.4087	19.7005	0.7676
	TBT	4.8285	1.6597	4.9924	0.7504	4.4644	0.4087	19.7004	0.7620
	SBT	4.8278	1.6613	4.9970	0.7720	4.4644	0.4087	19.7015	0.7855
	HBT	4.8285	1.6595	4.9920	0.7484	4.4644	0.4087	19.7003	0.7599
	EBT	4.8260	1.6628	5.0012	0.7934	4.4643	0.4088	19.7026	0.8089
	CBT	4.4401	1.6331	4.9206	-	4.4401	0.4083	19.6825	-
1	Li et al. [22]	6.2599	2.3045	5.8837	0.7500	5.8049	0.5686	23.2054	0.7500
	TBT	6.2594	2.3038	5.8836	0.7332	5.8049	0.5686	23.2053	0.7451
	SBT	6.2586	2.3058	5.8892	0.7549	5.8049	0.5686	23.2067	0.7686
	HBT	6.2594	2.3036	5.8831	0.7312	5.8049	0.5685	23.2052	0.7429
	EBT	6.2563	2.3075	5.8943	0.7763	5.8047	0.5686	23.2080	0.7920
	CBT	5.7746	2.2722	5.7959	-	5.7746	0.5680	23.1834	-
2	Li et al. [22]	8.0602	3.1134	6.8812	0.6787	7.4415	0.7691	27.0989	0.6787
	TBT	8.0677	3.1130	6.8826	0.6706	7.4421	0.7691	27.0991	0.6824
	SBT	8.0683	3.1153	6.8901	0.6933	7.4421	0.7692	27.1010	0.7069
	HBT	8.0675	3.1127	6.8819	0.6685	7.4420	0.7691	27.0989	0.6802
	EBT	8.0667	3.1174	6.8969	0.7157	7.4420	0.7692	27.1027	0.7315
	CBT	7.4003	3.0740	6.7676	-	7.4003	0.7685	27.0704	-
5	Li et al. [22]	9.7802	3.7089	8.1030	0.5790	8.8151	0.9133	31.8112	0.5790
	TBT	9.8281	3.7100	8.1106	0.5905	8.8182	0.9134	31.8130	0.6023
	SBT	9.8367	3.7140	8.1222	0.6155	8.8188	0.9134	31.8159	0.6292
	HBT	9.8271	3.7097	8.1095	0.5883	8.8181	0.9134	31.8127	0.5998
	EBT	9.8414	3.7177	8.1329	0.6404	8.8191	0.9135	31.8185	0.6562
	CBT	8.7508	3.6496	7.9428	-	8.7508	0.9124	31.7711	-
10	Li et al. [22]	10.8979	3.8860	9.7063	0.6436	9.6879	0.9536	38.1372	0.6436
	TBT	10.9381	3.8864	9.7122	0.6467	9.6905	0.9536	38.1385	0.6596
	SBT	10.9420	3.8913	9.7238	0.6708	9.6908	0.9537	38.1414	0.6858
	HBT	10.9375	3.8859	9.7111	0.6445	9.6905	0.9536	38.1383	0.6572
	EBT	10.9404	3.8957	9.7341	0.6944	9.6907	0.9538	38.1440	0.7115
	CBT	9.6072	3.8097	9.5228	-	9.6072	0.9524	38.0913	-

Table 3. Nondimensional fundamental frequency \tilde{S} of FG beams

L/h	Theory	Method	p					
			0	0.5	1	2	5	10
5	TBT	Simsek [23]	5.1527	4.4111	3.9904	3.6264	3.4012	3.2816
		Present	5.1527	4.4107	3.9904	3.6264	3.4012	3.2816
	SBT	Simsek [23]	5.1531	4.4114	3.9907	3.6263	3.3998	3.2811
		Present	5.1531	4.4110	3.9907	3.6263	3.3998	3.2811
	HBT	Simsek [23]	5.1527	4.4111	3.9904	3.6265	3.4014	3.2817
		Present	5.1527	4.4107	3.9904	3.6265	3.4014	3.2817
	EBT	Simsek [23]	5.1542	4.4122	3.9914	3.6267	3.3991	3.2813
		Present	5.1542	4.4118	3.9914	3.6267	3.3991	3.2814
	CPT	Simsek [23]	5.3953	4.5936	4.1484	3.7793	3.5949	3.4921
		Present	5.3953	4.5931	4.1484	3.7793	3.5949	3.4921
20	TBT	Simsek [23]	5.4603	4.6516	4.2050	3.8361	3.6485	3.5390
		Present	5.4603	4.6511	4.2051	3.8361	3.6485	3.5390
	SBT	Simsek [23]	5.4604	4.6516	4.2051	3.8361	3.6484	3.5390
		Present	5.4603	4.6511	4.2051	3.8361	3.6484	3.5389
	HBT	Simsek [23]	5.4603	4.6516	4.2050	3.8361	3.6485	3.5390
		Present	5.4603	4.6511	4.2051	3.8361	3.6485	3.5390
	EBT	Simsek [23]	5.4604	4.6517	4.2052	3.8362	3.6483	3.5390
		Present	5.4604	4.6512	4.2051	3.8361	3.6483	3.5390
	CPT	Simsek [23]	5.4777	4.6646	4.2163	3.8472	3.6628	3.5547
		Present	5.4777	4.6641	4.2163	3.8472	3.6628	3.5547

Table 4. First three nondimensional frequencies $\tilde{\omega}$ of FG beams

L/h	Mode	Method	$\tilde{\omega}$					
			0	0.5	1	2	5	10
5	1	TBT	5.1527	4.4107	3.9904	3.6264	3.4012	3.2816
		SBT	5.1531	4.4110	3.9907	3.6263	3.3998	3.2811
		HBT	5.1527	4.4107	3.9904	3.6265	3.4014	3.2817
		EBT	5.1542	4.4118	3.9914	3.6267	3.3991	3.2814
		CBT	5.3953	4.5931	4.1484	3.7793	3.5949	3.4921
	2	TBT	17.8812	15.4588	14.0100	12.6405	11.5431	11.0240
		SBT	17.8868	15.4631	14.0138	12.6411	11.5324	11.0216
		HBT	17.8810	15.4587	14.0098	12.6407	11.5444	11.0246
		EBT	17.8996	15.4728	14.0224	12.6466	11.5281	11.0264
		CBT	20.6187	17.5415	15.7982	14.3260	13.5876	13.2376
	3	TBT	34.2097	29.8382	27.0979	24.3152	21.7158	20.5561
		SBT	34.2344	29.8569	27.1152	24.3237	21.6943	20.5581
		HBT	34.2085	29.8373	27.0971	24.3151	21.7187	20.5569
		EBT	34.2819	29.8929	27.1480	24.3482	21.6924	20.5815
		CBT	43.3483	36.8308	33.0278	29.7458	28.0850	27.4752
20	1	TBT	5.4603	4.6511	4.2051	3.8361	3.6485	3.5390
		SBT	5.4603	4.6511	4.2051	3.8361	3.6484	3.5389
		HBT	5.4603	4.6511	4.2051	3.8361	3.6485	3.5390
		EBT	5.4604	4.6512	4.2051	3.8361	3.6483	3.5390
		CBT	5.4777	4.6641	4.2163	3.8472	3.6628	3.5547
	2	TBT	21.5732	18.3962	16.6344	15.1619	14.3746	13.9263
		SBT	21.5736	18.3965	16.6347	15.1617	14.3728	13.9255
		HBT	21.5732	18.3962	16.6344	15.1619	14.3748	13.9264
		EBT	21.5748	18.3974	16.6355	15.1621	14.3718	13.9258
		CBT	21.8438	18.5987	16.8100	15.3334	14.5959	14.1676
	3	TBT	47.5930	40.6526	36.7679	33.4689	31.5780	30.5369
		SBT	47.5950	40.6542	36.7692	33.4681	31.5699	30.5337
		HBT	47.5930	40.6526	36.7679	33.4691	31.5789	30.5373
		EBT	47.6008	40.6586	36.7730	33.4701	31.5655	30.5349
		CBT	48.8999	41.6328	37.6173	34.2954	32.6357	31.6883